A tunable microcavity

Russell J. Barbour, Paul A. Dalgarno, Arran Curran, Kris M. Nowak, Howard J. Baker et al.

Related Articles

Achieving all-dielectric left-handed metamaterials via single-sized dielectric resonators
J. Appl. Phys. 111, 044903 (2012)

Design, fabrication and measurement of a broadband polarization-insensitive metamaterial absorber based on lumped elements
J. Appl. Phys. 111, 044902 (2012)

Analysis and experimental demonstration of an active acoustic metamaterial cell
J. Appl. Phys. 111, 044505 (2012)

Circular multilayer zone plate for high-energy x-ray nano-imaging
Rev. Sci. Instrum. 83, 013705 (2012)

Tunneling and filtering characteristics of cascaded -negative metamaterial layers sandwiched by double-positive layers
J. Appl. Phys. 111, 014906 (2012)

Additional information on J. Appl. Phys.

Journal Homepage: http://jap.aip.org/

Journal Information: http://jap.aip.org/about/about_the_journal

Top downloads: http://jap.aip.org/features/most_downloaded

Information for Authors: http://jap.aip.org/authors

ADVERTISEMENT

A tunable microcavity

Russell J. Barbour,[1] Paul A. Dalgarno,[1] Arran Curran,[1] Kris M. Nowak,[1] Howard J. Baker,[1]
Denis R. Hall,[1] Nick G. Stoltz,[2] Pierre M. Petroff,[2] and Richard J. Warburton[1,3,a]

[1]*School of Engineering and Physical Sciences, Heriot-Watt University, Edinburgh EH14 4AS, United Kingdom*
[2]*Materials Department, University of California, Santa Barbara, California 93106, USA*
[3]*Department of Physics, University of Basel, Klingelbergstrasse 82, Basel 4056, Switzerland*

We present a generic microcavity platform for cavity experiments on optically active nanostructures, such as quantum dots, nanocrystals, color centers, and carbon nanotubes. The cavity is of the Fabry-Pérot type with a planar back mirror and a miniature concave top mirror with radius of curvature $\sim 100\ \mu$m. Optical access is achieved by free beam coupling, allowing good mode-matching to the cavity mode. The cavity has a high Q-factor, reasonably small mode volume, open access, spatial and spectral tunability, and operates at cryogenic temperatures. Spectral and spatial tuning of the Purcell effect (weak coupling regime) on a single InGaAs quantum dot is demonstrated. © *2011 American Institute of Physics*. [doi:10.1063/1.3632057]

A microcavity can increase massively the interaction of light with a single nanostructure and is a key component in the quantum photonics toolbox.[1] In the weak coupling regime, a photon emitted by an optically-active nanostructure, such as a quantum dot, leaks out before it is reabsorbed. Nevertheless, the emitted photons are funneled efficiently into the cavity mode, and spontaneous emission is accelerated on account of the increased density of states: the Purcell effect.[2,3] Weak coupling increases the quantum efficiency and the device repetition rate of a single photon source.[4] In the strong coupling regime, a photon is reabsorbed by the nanostructure before it leaks out and new eigenstates are formed: coherent admixtures of atom and photon.[5–10] Strong coupling enables the entangling of remote qubits via a common interaction with the photon.[11]

The majority of successful microcavity experiments on nanostructures have been performed so far on self-assembled quantum dots. Both weak coupling[2,3] and strong coupling have been observed.[5–9] The properties of other optically active nanostructures, for instance, color centers in diamond,[10,12–14] carbon nanotubes,[15] and semiconductor nanocrystals[16] also benefit from a resonant microcavity. Independent of the particular nanostructure, exploiting cavity effects requires that the cavity mode and the emitter must be precisely aligned. The problem is two-fold. First, the anti-node of the cavity mode must be located at the position of the nanostructure, and second, the cavity mode wavelength must match the nanostructure emission wavelength.[1] For self-assembled quantum dots, the work-horse geometries are micropillars, photonic crystal micro-cavities, and whispering gallery devices.[1] With these microcavities, *in situ* spatial tuning is ruled out and there are only limited possibilities for *in situ* spectral tuning. Recently, techniques have been developed to construct the cavity around a particular quantum dot.[17,18] Nevertheless, once the cavity is constructed, there is no possibility for *in situ* spatial tuning. Spectral tuning is very important in quantum

dot devices: at low temperature, the optical quantum dot linewidth is just a few μeV and the cavity mode linewidth in high Q devices approaches $\sim 10\ \mu$eV. For monolithic quantum dot microcavities, each technique for *in situ* spectral tuning has a limitation. Temperature tuning requires heating up to ~ 50 K to achieve even a few meV shift of the exciton,[5] and at these temperatures, the exciton is dephased rapidly by the phonons. Adsorption of gases to the etched surfaces of a photonic crystal at low temperature leads to some spectral tuning, but it is slow and irreversible.[8] Improvements in processing have recently enabled a p-i-n diode to be incorporated into both a micropillar[19] and photonic crystal microcavity,[20] allowing the quantum dot energy to be tuned via the quantum-confined Stark effect and the quantum dot charge to be controlled with Coulomb blockade,[21] but only tunings of a few meV can be achieved before field ionization takes place. Furthermore, these monolithic microcavity geometries do not translate easily to other nanostructures.

We present here a generic microcavity with high Q-factor, reasonably small mode volume, open access, and spatial and spectral tunability. The cavity is of the Fabry-Pérot type,[22–26] but highly miniaturized, allowing both a high Q-factor and small mode volume. We employ a planar back mirror and a miniature concave top mirror. A similar microfabrication procedure as for "fiber cavities" is adopted,[25,26] but instead of using a fiber, the setup has free-beam coupling, allowing good mode matching to the cavity mode. We demonstrate spectral and spatial tuning of the Purcell effect on a single quantum dot. We argue that improving the microcavity Q-factor with existing dielectric mirror technology should allow several coherent quantum dot-photon oscillations before dephasing.

The tunable micro-cavity is shown schematically in Fig. 1(a). A miniaturized plane-spherical cavity contains a stable cavity mode. The bottom mirror is a distributed Bragg reflector (DBR), in this case, part of the semiconductor heterostructure. Above the DBR is the optically active layer, here, self-assembled quantum dots. The top mirror is a dielectric DBR deposited onto a concave template in a silica substrate.

110, 053107-1
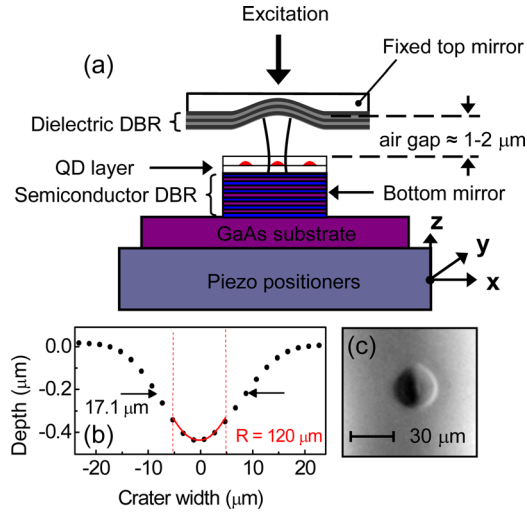© 2011 American Institute of Physics

FIG. 1. (Color online) Schematic of a fully tunable microcavity for a quantum dot experiment. (a) The bottom mirror is a semiconductor distributed Bragg reflector (DBR) and the active layer contains self-assembled quantum dots. The top mirror is a miniature concave template coated with a dielectric DBR. The bottom mirror can be moved in x and y, allowing spatial tuning of the cavity anti-node with respect to a single quantum dot, and in z, allowing spectral tuning of the cavity. (b) Profile of a crater created in a silica substrate with laser ablation measured using a stylus surface profiler. The curve is a fit to a spherical section with radius of curvature, $R = 120$ μm. (c) Optical microscope image of the crater.

Spatial tuning is achieved by moving the bottom mirror with respect to the top mirror in the lateral (x, y) plane; spectral tuning is achieved by moving the bottom mirror in the z direction. Light can be coupled in and out of the cavity via a free optical beam above the top mirror. By focusing a beam with the appropriate numerical aperture, good mode matching can be achieved. The beam emerging from the microcavity is conveniently a Gaussian beam.

Diffraction limits the mode area in a cavity with very small radius of curvature to $\sim\lambda^2$. However, when the cavity length L is much smaller than the radius of curvature of the mirror, R, the mode area increases proportional to $\sqrt{R}$, a gentle dependence on R. This means that cavity mode areas approaching the diffraction limit can be achieved, even when R is substantially larger than the wavelength, λ. Here, $\lambda \sim 1$ μm and $R \sim 100$ μm and the full-width-at-half-maximum (FWHM) of the fundamental cavity mode is ~ 3 μm. Equations for the microcavity's vital statistics can be developed. In the limit that the cavity length L is small ($L \ll R$), the lateral mode area is $A = \frac{\lambda_o}{2}\sqrt{LR}$, where λ_o is the free space wavelength. In the longitudinal direction, the cavity is formed by a top dielectric DBR and a bottom semiconductor DBR. The light penetrates much further into the semiconductor DBR (penetration length L^s_{DBR}) than the dielectric DBR (penetration length L^d_{DBR}) such that the cavity length $L \simeq L^s_{\mathrm{DBR}} + \frac{\lambda_o}{n} + L_{\mathrm{air}} + L^d_{\mathrm{DBR}} \simeq 2\lambda_o + L_{air}$. ($n$ is the refractive index of GaAs, L_{air} is the air gap thickness, and the dots are embedded at the center of a λ-layer.) The energy of the vacuum field mode is stored largely in the semiconductor over a length $\simeq \lambda_o/n$ such that the mode volume is $V \simeq \frac{\lambda_o^2}{2n}\sqrt{LR}$. The electric field associated with the vacuum field can then be estimated by $E_{\mathrm{vac}} = \sqrt{\frac{\hbar\omega_o}{2\epsilon_o n^2 V}}$, where ε_o is the

permittivity of free space and $\hbar\omega_o$ is the photon energy. This large vacuum electric field accelerates spontaneous decay, provided the quantum dot is in a spatial and spectral resonance with the cavity. In resonance, the decay rate is $\gamma = \frac{2\pi}{\hbar^2}\mu_{12}^2 E_{\mathrm{vac}}^2 g(\omega_o)$, where μ_{12} is the matrix element of the optical dipole and g is the density of states. Once the cavity mode is sufficiently narrow, there is a coherent coupling between the quantum dot and the cavity with energy splitting at the bare quantum dot energy of $E_{\mathrm{Rabi}} = 2\mu_{12}E_{\mathrm{vac}}$.

The concave template is created with laser ablation, a process which transfers the intensity profile of a laser beam into a spatial profile in the substrate. We exploit the high absorption of a silica substrate to 10.6 μm wavelength radiation. The single mode output of a temperature stabilized CO_2 laser is focused with a ZnSe lens (focal length 3.81 mm) onto a silica substrate. A single 70 μs, 25 Jcm^{-2} pulse produces a concave template (see Fig. 1(b) and (c)), with a depth of 500 nm, diameter of 30 μm, and radius of curvature in the crater bottom, $R = 120$ μm. The surface roughness is less than 0.3 nm: the surface tension of the molten glass pulls out any surface irregularities. By adjusting the position of the silica substrate relative to the focus, we were able to vary the diameter from 27 to 59 μm. The resulting R lies between 80 and 150 μm; a smaller R can probably be created by a smaller focal spot. An array of craters was fabricated on a flat silica substrate, and the entire substrate was then coated with ten pairs of TiO_2 (refractive index $n = 2.25$), SiO_2 ($n = 1.45$) $\lambda/4$ layers. The final layer was SiO_2. The predicted reflectivity, assuming zero losses, is $R = 99.9\%$. The advantage of the setup over a fiber cavity [24–26] is that, first, mode matching of the propagating and cavity modes can be achieved, even when the cavity mode is highly confined, and second, the concave mirror can be changed *in situ* by moving from one crater in the array to another.

The semiconductor sample was grown by molecular beam epitaxy. The DBR mirror consists of 32 pairs of AlGaAs ($n = 3.009$), GaAs ($n = 3.54$) $\lambda/4$ layers with a target wavelength of $\lambda = 950$ nm. The predicted reflectivity, assuming zero losses, is $R = 99.99\%$. On top of the final AlGaAs layer, there is a $\lambda/2$ GaAs, followed by the InGaAs quantum dots, and a final $\lambda/2$ layer. The sample is mounted on a positioning unit consisting of an x, y scanner allowing a 12×12 μm^2 scan area at 4 K and a z slip-slide positioner. This unit is mounted on a U-shaped part, on top of which the curved mirror is mounted face down to complete the microcavity. The z positioner allows both a coarse approach of the sample with respect to the fixed mirror and then fine control once a suitable cavity length has been reached. The entire microcavity is then mounted on a three-axis slip-slide positioning system and cooled to 4 K in a bath cryostat. Once cold, for the Q-factors achieved here, the system proved to be sufficiently insensitive to mechanical noise and drift that active cavity stabilization was not required. A free space collimated beam is coupled to the cavity mode via an aspheric lens with numerical aperture 0.55, the slip-slide positioners allowing the microcavity to be positioned relative to the beam's focus.

The cavity was characterized at room temperature by coupling in a 950-nm wavelength laser, measuring the transmission as a function of voltage applied to the cavity z-piezo.
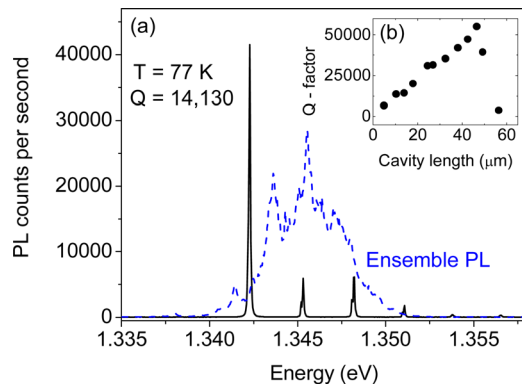
FIG. 2. (Color online) Optical characterization of the tunable microcavity. (a) Photoluminescence (PL) from a high density ensemble of quantum dots located inside the microcavity at 77 K plotted against energy (solid line). One longitudinal mode exists within the bandwidth of the quantum dot PL; accompanying the main peak corresponding to emission into the mode with lateral mode index $m + n = 0$ is a series of lateral modes with $m + n = 1$, 2, 3. m and n are the mode indices: the number of anti-nodes in the lateral field distribution [Ref. 27]. The ensemble PL of the dots recorded from a piece of bare wafer without the top mirror cavity is also shown (dashed line). The spectral resolution of the spectrometer system is 70 μeV. (b) Cavity Q as a function of cavity length.

Once the beam is focused onto the center of a crater, a series of narrow cavity modes appears. The highest cavity finesse we have achieved with this mirror set is 1500. At 77 K, we characterize the microcavity by using the quasi-continuous photoluminescence (PL) spectrum from a high density quantum dot sample as an internal light source. Light emerges from the cavity at the cavity mode energies (see Fig. 2). The spectral separation of the modes in Fig. 2 can be used to determine the radius of curvature of the concave mirror, $R = 110$ μm, agreeing well with the measured curvature before coating, $R = 120$ μm. As expected, Q depends on the cavity length: with a finesse of 900 in this particular case,

$Q = 5000$ for short cavity lengths, rising to $Q = 55\,000$ at cavity length $L = 45$ μm (see Fig. 2). Further increases in L cause the Q-factor to plummet. This corresponds closely to the instability point at $L = R$.[27]

At 4.2 K, the quantum dot PL spectrum breaks up into discrete lines, each one from an individual quantum dot. Figure 3 shows how the microcavity PL spectrum depends on the microcavity length. Emission into the cavity modes is always present, but at specific energies, emission into the fundamental mode increases significantly (see Fig. 3(a) and (c)). Each resonance corresponds to an interaction with a single quantum dot. Figure 3(a) shows also emission into the first lateral mode, but there is only a small enhancement at the resonances with the quantum dots. This confirms that the dots are located close to the node of the first lateral mode, equivalently, the anti-node of the fundamental mode. Emission at the cavity mode exists to wavelengths right out to 980 nm (the long wave-length limit of the silicon detector), wavelengths considerably larger than the emission of even the reddest dot in the ensemble. Similar behavior has been observed also in photonic crystal[8] and micropillar devices,[28] arising in all likelihood as a consequence of the exciton-acoustic phonon interaction.

To demonstrate that the behavior in Fig. 3 signifies more than spectral filtering, we measured the radiative decay rates as the cavity is spatially centered on a particular quantum dot and then spectrally tuned through the resonance. A spectrally isolated dot was chosen for these experiments (see Fig. 3(b)). Figure 4(a) shows a decay curve on resonance (radiative lifetime 0.38 ns); Fig. 4(b) shows a decay curve 0.5 nm (700 μeV) spectrally detuned (radiative lifetime 1.2 ns). Figure 4(c) shows the full dependence of the radiative lifetime on the spectral detuning of the cavity at the spatial resonance. There is clear proof that the radiative lifetime is decreased on resonance. Furthermore, the radiative lifetime
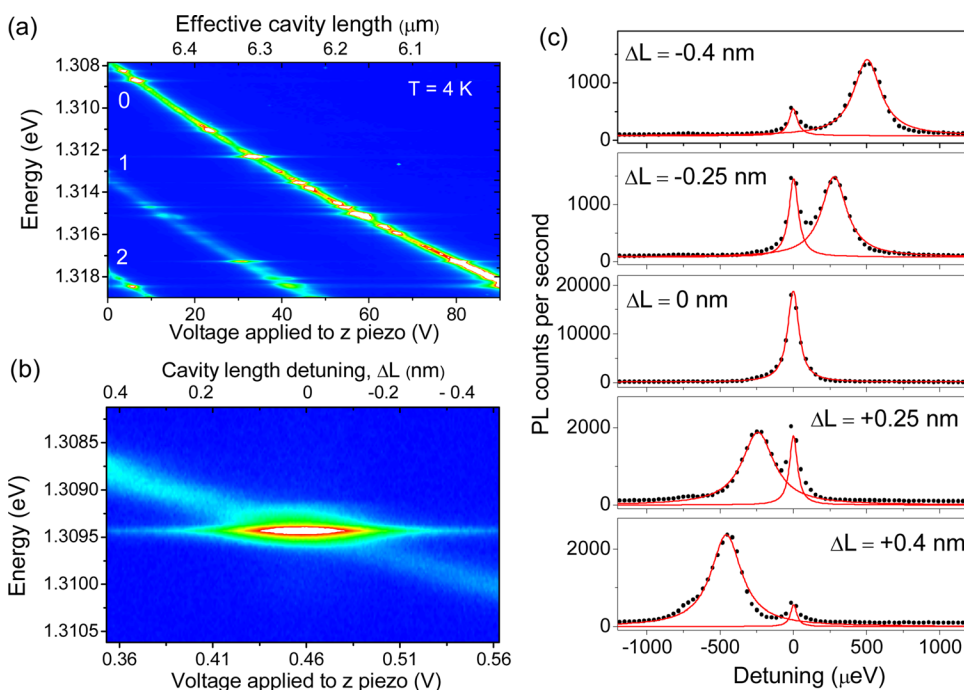

FIG. 3. (Color online) Quantum dot photoluminescence (PL) as a function of microcavity detuning at 4.2 K. The PL was excited non-resonantly with a laser with wavelength 830 nm. The cavity anti-node was adjusted to coincide with the quantum dot. (a) PL vs microcavity length (background representing 0 counts, white 30 000 counts). The modes are labeled with the lateral mode index $m + n$. (b) PL versus microcavity length showing a pronounced resonance with one particular quantum dot. (c) PL spectra for several cavity detunings close to the resonance using the data in (b). The curves are fits to two Lorentzians.
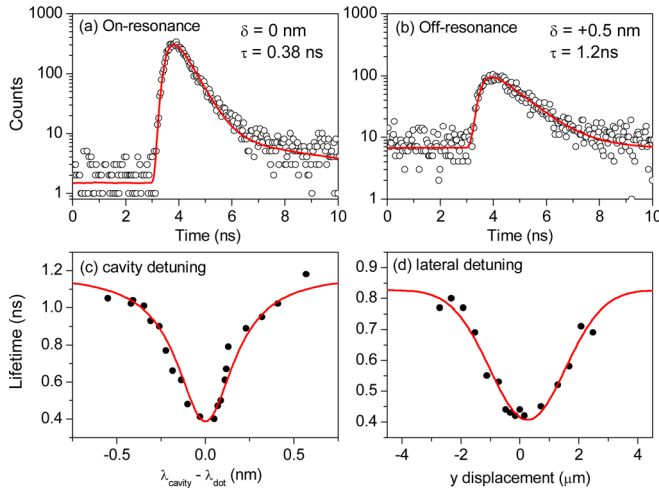
FIG. 4. (Color online) Lifetime measurements from a single quantum dot in the tunable microcavity at 4.2 K. The same dot and cavity setup were used as in Fig. 3(b). The PL was excited with 50 ps pulses from an 830 nm laser. Decay curves were recorded with timing resolution 500 ps using a silicon avalanche photodetector and time-correlated single photon counting. (a) Decay curve at the spatial and spectral resonance; (b) decay curve at the spatial resonance but spectrally detuned by wavelength 0.5 nm. The curves are the result of a fit taking into account the response of the detector. (c) Lifetime at the spatial resonance as a function of spectral (wavelength) detuning with a Lorentzian fit with FWHM 0.25 nm. (d) Lifetime at the spectral resonance as a function of spatial detuning with a Gaussian fit with FWHM 2.5 μm.

away from resonance, 1.2 ns, is considerably larger than the average radiative lifetime of a typical dot grown with the same protocol at this wavelength, 0.8 ± 0.2 ns,[29] evidence that the radiative lifetime is increased above the free space value away from the spectral resonance with the cavity mode. These results constitute a demonstration of the Purcell effect in the tunable microcavity. We fit the data to

$$\frac{\gamma_{\text{cav}}}{\gamma_{\text{free}}} = \frac{F_p \Delta^2}{4(\lambda_X - \lambda_c)^2 + \Delta^2} + \alpha, \qquad (1)$$

where the first term describes the density of states of the cavity mode and the second term describes the relative decay rate into leaky modes associated with emission at large angles from the vertical.[2,3] γ_{cav} is the decay rate in the cavity, γ_{free} is the decay rate in free space, F_p is the Purcell factor, λ_X is the wavelength of the quantum dot exciton, λ_c is the wavelength of the cavity mode, and Δ is the spectral width in wavelength of the cavity mode. Taking $\gamma_{\text{free}} = 1.25$ GHz (radiative decay time 0.8 ns), a good fit is obtained with $\Delta = 0.21$ nm (implying $Q = 4500$), $F_p = 1.6$, and $\alpha = 0.7$ (see Fig. 4(c)). Good fits are possible over the range of possible γ_{free}, an increase in F_p accompanied by an increase in α. Allowing for the uncertainty in γ_{free}, we can conclude that $F_p = 1.6 \pm 0.4$, $\alpha = 0.7 \pm 0.2$. α is less than one, indicating that the coupling to the continuum of lateral modes (the "leaky" modes) is inhibited by the cavity; this is not the case for uncoated micropillars.[2,3] At large detunings, γ_{cav} is dominated by the α term: emission is almost entirely into the lateral continuum such that, at large detunings, the measured PL intensity is small (see Fig. 3).

Figure 4(c) demonstrates spectral tuning of the microcavity. To demonstrate also spatial tuning, we recorded the radiative decay time as a function of lateral position (x,y) while maintaining the spectral resonance (see Fig. 4(d)). The radiative decay time is smallest at $x, y = 0$, increasing as the cavity anti-node is displaced with respect to the quantum dot. We fit the spatial detuning curve to a Gaussian (see Fig. 4(d)), and for both x and y, the FHWM is 3.0 μm. This provides a measure of the lateral diameter of the fundamental cavity mode. It corresponds well to the value expected according to Gaussian optics: for $R = 120$ μm, $L = 4.75$ μm, $\lambda = 950$ nm, the mode has a lateral FWHM of 2.8 μm.

We speculate on the future possibilities of this technology for single InGaAs quantum dots. To calculate the Purcell factor and also predict Rabi energies in the limit of strong coupling, we assume that the axial and lateral field profiles can be separated. Given the very small beam expansion over the extent of the microcavity, this is a good approximation. We take a Gaussian mode in the lateral direction with a realistic FWHM of 3.0 μm. We calculate the standing wave in the longitudinal direction with a transfer matrix, insisting that the sum of the vacuum field energy equals the zero point energy. Assuming perfect layers (negligible absorption and zero scattering), we find that 84% of the vacuum energy is stored in the semiconductor, just 11% in the dielectric and 5% in the air gap, and that the vacuum electric field at the location of the dot is $E_{\text{vac}} = 1.57 \times 10^6$ V/cm. The approximate result for E_{vac} calculated using the estimate of the cavity mode volume gives a very similar result. The transfer matrix model also predicts $Q = 83\,000$. In the experiment, imperfections, most likely in the upper DBR, reduce Q to 4500. This is a large decrease, but nevertheless, Q remains high and we therefore assume that, in the real cavity, E_{vac} is given approximately by the ideal limit. Taking a randomly oriented dipole, we calculate a Purcell factor $F_p = 4.0$. This is in rough agreement with the experiment; a better calculation would include the deficiencies in the top mirror, which are not known to us with any precision. A free space radiative lifetime of 0.8 ns translates into an optical dipole moment of $\mu_{12} = 1.2$ nm. When the cavity and quantum dot exchange energy coherently, the strong coupling regime, the splitting is $E_{\text{Rabi}} = 2\mu_{12}E_{\text{vac}}$. For the present experiment, the calculated E_{vac} results in $E_{\text{Rabi}} = 38$ μeV. This is too small to be observed: the experimental $Q = 4500$ results in a cavity mode linewidth of 290 μeV. However, if the mirrors had ideal behavior, the cavity mode linewidth would reduce to 16 μeV and strong coupling would be evident. This limit is within easy reach using high quality dielectric layers. However, the goal is to achieve many coherent oscillations before the system dephases, equivalently, a large Rabi splitting compared to the cavity mode and quantum dot linewidths. This has not yet been achieved for a single quantum dot and will not be straightforward with this miniaturized Fabry-Pérot. However, we point out a number of possible advantages of this technology. First, the mode waist can be decreased without a reduction in Q, unlike micropillars, for which Q decreases as the micropillar diameter is decreased below about 2 μm, owing to scattering at the etched surface. Secondly, the use of high quality dielectric mirrors can provide a massive boost to Q. The micromirrors in the cold atom experiment[25] would give $Q = 4 \times 10^5$ in this experiment; Q can be increased by a further order of magnitude using

"supermirrors".[30] Thirdly, the full tunability enables the high Q cavity modes to be exploited: in a monolithic device, it becomes increasingly difficult to match the quantum dot and cavity mode energies by fabrication techniques alone as the cavity linewidth decreases. We consider a quantum dot in a high Q tunable microcavity. Quantum dot linewidths as low as 2 μeV are routinely achieved.[31] For a radiative lifetime of 0.33 ns and energy 1.3 eV, radiatively broadened exciton lines are possible, and we consider a cavity with sufficiently high quality mirrors such that the quantum dot and cavity mode linewidths are matched at 2.0 μeV (cavity $Q = 6.5 \times 10^5$). Taking $R = 50$ μm, a dielectric top DBR and a semiconductor bottom DBR, E_{Rabi} increases to 71 μeV, 36 times larger than the quantum dot and cavity linewidths. This ratio can be increased to about 50 by using high quality dielectric mirrors top and bottom. We note that the large splitting-to-linewidth ratio is predicted based on *existing* quantum dot linewidth, mirror radius, and dielectric mirror quality. This analysis suggests that the tunable microcavity provides a promising route to performing cavity QED experiments on single dots.

In conclusion, we report the observation of the Purcell effect on a single self-assembled quantum dot in a miniaturized Fabry-Pérot cavity. We argue that the spatial plus spectral tunability and the open access are attractive features for cavity experiments on a wide range of optically active nanostructures.

[1]K. J. Vahala, Nature **424**, 839 (2003).

[2]J. M. Gérard, B. Sermage, B. Gayral, B. Legrand, E. Costard, and V. Thierry-Mieg, Phys. Rev. Lett. **81**, 1110 (1998).

[3]M. Bayer, T. L. Reinecke, F. Weidner, A. Larionov, A. McDonald, and A. Forchel, Phys. Rev. Lett. **86**, 3168 (2001).

[4]S. Strauf, N. G. Stoltz, M. T. Rakher, L. A. Coldren, P. M. Petroff, and D. Bouwmeester, Nature Photonics **1**, 704 (2007).

[5]J. P. Reithmaier, G. Sek, A. Löffler, C. Hofmann, S. Kuhn, S. Reitzenstein, L. V. Keldysh, V. D. Kulakovskil, T. L. Reinecke, and A. Forchel, Nature **432**, 197 (2004).

[6]T. Yoshie, A. Scherer, J. Hendrickson, G. Khitrova, H. M. Gibbs, G. Rupper, C. Ell, O. B. Shchekin, and D. G. Deppe, Nature **432**, 200 (2004).

[7]E. Peter, P. Senellart, D. Martrou, A. Lemaître, J. Hours, J. M. Gerard, and J. Bloch, Phys. Rev. Lett. **95**, 067401 (2005).

[8]K. Hennessy, A. Badolato, M. Winger, D. Gerace, M. Atatüre, S. Gulde, S. Fält, E. L. Hu, and A. Imamoglu, Nature **445**, 896 (2007).

[9]K. Srinivasan and O. Painter, Nature **450**, 862 (2007).

[10]Y. S. Park, A. K. Cook, and H. Wang, Nano Lett. **6**, 2075 (2006).

[11]A. Imamoglu, D. D. Awschalom, G. Burkard, D. P. DiVincenzo, D. Loss, M. Sherwin, and A. Small, Phys. Rev. Lett. **83**, 4204 (1999).

[12]M. Larsson, K. N. Dinyari, and H. Wang, Nano Lett. **9**, 1447 (2009).

[13]C. H. Su, A. D. Greentree, and L. C. L. Hollenberg, Opt. Express **16**, 6240 (2007).

[14]A. Young, C. Y. Hu, L. Marseglia, J. P. Harrison, J. L. O'Brien, and J. G. Rarity, New J. Phys. **11**, 013007 (2009).

[15]F. N. Xia, M. Steiner, Y. M. Lin, and P. Avouris, Nat. Nanotechnol. **3**, 609 (2008).

[16]M. Kahl, T. Thomay, V. Kohnle, K. Beha, J. Merlein, M. Hagner, A. Halm, J. Ziegler, T. Nann, Y. Fedutik, U. Woggon, M. Artemyev, F. Pérez-Willard, A. Leitenstorfer, and R. Bratschitsch, Nano Lett. **7**, 2897 (2007).

[17]A. Badolato, K. Hennessy, M. Atature, J. Dreiser, E. Hu, P. M. Petroff, and A. Imamoglu, Science **308**, 5725 (2005).

[18]A. Dousse, L. Lanco, J. Suffczynski, E. Semenova, A. Miard, A. Lemaître, I. Sagnes, C. Roblin, J. Bloch, and P. Senellart, Phys. Rev. Lett. **101**, 267404 (2008).

[19]C. Kistner, T. Heindel, C. Schneider, A. Rahimi-Iman, S. Reitzenstein, S. Höfling, and A. Forchel, Optics Express **16**, 15006 (2008).

[20]A. Laucht, F. Hofbauer, N. Hauke, A. Angele, S. Stobbe, M. Kaniber, G. Böhm, P. Lodahl, M.-C. Amann, and J. J. Finley, New J. Physics **11**, 023034 (2009).

[21]M. T. Rakher, N. Stoltz, L. A. Coldren, P. M. Petroff, and D. Bouwmeester, Phys. Rev. Lett. **102**, 097403 (2009).

[22]M. Trupke, E. A. Hinds, S. Eriksson, E. A. Curtis, Z. Moktadir, E. Kukharenka, and M. Kraft, Appl. Phys. Lett. **87**, 211106 (2005).

[23]G. Cui, J. M. Hannigan, R. Loeckenhoff, F. M. Matinaga, M. G. Raymer, S. Bhongale, M. Holland, S. Mosor, S. Chatterjee, H. M. Gibbs, and G. Khitrova, Optics Express **14**, 2289 (2006).

[24]T. Steinmetz, Y. Colombe, D. Hunger, T. W. Hänsch, A. Balocchi, R. J. Warburton, and J. Reichel, Appl. Phys. Lett. **89**, 111110 (2006).

[25]Y. Colombe, T. Steinmetz, G. Dubois, F. Linke, D. Hunger, and J. Reichel, Nature **450**, 272 (2007).

[26]A. Muller, E. B. Flagg, M. Metcalfe, J. Lawall, and G. S. Solomon, Appl. Phys. Lett. **95**, 173101 (2009).

[27]A. Yariv, *Optical Electronics in Modern Communications* (Oxford University Press, Oxford, 1997).

[28]D. Press, S. Götzinger, S. Reitzenstein, C. Hofmann, A. Löffler, M. Kamp, A. Forchel, Y. Yamamoto, Phys. Rev. Lett. **98**, 117402 (2007).

[29]P. A. Dalgarno, J. M. Smith, J. McFarlane, B. D. Gerardot, K. Karrai, A. Badolato, P. M. Petroff, and R. J. Warburton, Phys. Rev. B **77**, 245311 (2008).

[30]C. J. Hood, T. W. Lynn, A. C. Doherty, A. S. Parkins, and H. J. Kimble, Science **287**, 1447 (2000).

[31]A. Högele, S. Seidl, M. Kroner, K. Karrai, R. J. Warburton, B. D. Gerardot, and P. M. Petroff, Phys. Rev. Lett. **93**, 217401 (2004).